

KenCoh: A Ranked-Based Canonical Coherence ¹

Mara Sherlin D.P. Talento^{a*}, Sarbojit Roy^{b*}, Hernando Ombao^{c*}

^a*marasherlin.talento@kaust.edu.sa*, ^b*sarbojit.roy@kaust.edu.sa*,

^c*hernando.ombao@kaust.edu.sa*

*Statistics Program, Computer Electrical and Mathematical Science & Engineering,
King Abdullah University of Science and Technology

Abstract

In this paper, we consider the problem of characterizing a robust global dependence between two brain regions where each region may contain several voxels or channels. This work is driven by experiments to investigate the dependence between two cortical regions and to identify differences in brain networks between brain states, e.g., alert and drowsy states. The most common approach to explore dependence between two groups of variables (or signals) is via canonical correlation analysis (CCA). However, it is limited to only capturing linear associations and is sensitive to outlier observations. These limitations are crucial because brain network connectivity is likely to be more complex than linear and that brain signals may exhibit heavy-tailed properties. To overcome these limitations, we develop a robust method, Kendall canonical coherence (KenCoh), for learning monotonic connectivity structure among neuronal signals filtered at given frequency bands. Furthermore, we propose the KenCoh-based permutation test to investigate the differences in brain network connectivity between two different states. Our simulation study demonstrates that KenCoh is competitive to the traditional variance-covariance estimator and outperforms the later when the underlying distributions are heavy-tailed. We apply our method to EEG recordings from a virtual-reality driving experiment. Our proposed method led to further insights on the differences of frontal-parietal cross-dependence network when the subject is alert and when the subject is drowsy and that left-parietal channel drives this dependence at the beta-band.

Keywords: canonical coherence; EEG; Kendall's tau; multivariate; robust; spectral analysis.

¹Preprint

1 Introduction

Millions suffer road traffic injuries each year, with driver behavior being a major contributing factor (Vecino-Ortiz et al., 2022). Thus, it is important to understand driver’s physiological brain behavior. One study revealed that the occipital and parietal brain regions are linked to driving collision avoidance, as these areas are responsible for processing visual information and spatial awareness (Spiers and Maguire, 2007). Shi et al. (2023) observed that the frontal cortical regions and prefrontal regions are highly activated when presented with visual and auditory cognitive distractions. These papers suggest that cortical regions, such as, occipital-parietal, frontal and pre-frontal regions, are responsible for our attention and cognition while driving. In this paper, we develop a statistical method that explores variation in connectivity between two brain regions for different brain conditions (e.g., drowsy and alert state). We analyze the driving data from Cao et al. (2019) to characterize the dynamics and brain connectivity structure between occipital-parietal region and frontal-prefrontal region when the driver is in alert-state and when the driver is in drowsy-state.

The dataset from Cao et al. (2019) consists of multiple electroencephalogram (EEG) recordings during a virtual-reality driving experiment with annotations on whether the driver is alert or drowsy. EEG is one of the non-invasive modalities in experimental studies which places multiple nodes on the scalp that are strategically designated to sample brain signals. Figure 2 shows ten EEG channels located on the scalp that are named after specific brain regions, i.e., blue colored nodes are channels on top of the frontal-prefrontal region and red colored nodes are channels on top of the occipital-parietal region. The mid pane of Figure 2 plots the extracted “oscillatory” signals (formally defined in Section 1.1) from the ten EEG channels of frontal-prefrontal and occipital-parietal lobe. Here, we can see high synchrony among signals sampled within the same brain region. The most common approach to network analysis in the literature involves examining pairwise connectivity between channels, with the aim of determining key aspects of brain functionality given a specific task (Bastos and Schoffelen, 2016). However, as discussed above, brain functionalities are mostly associated in the brain regions (or groups of channels) rather than between specific channel pairs. Moreover, there are concurrent dependence among signals within the same brain region that we may not capture if we analyze these signals by pair. Hence, interpretability of brain connections may be more sensible if seen at a larger scale, which is more consistent with the inherent spatial resolution of the EEG data. In this article, we

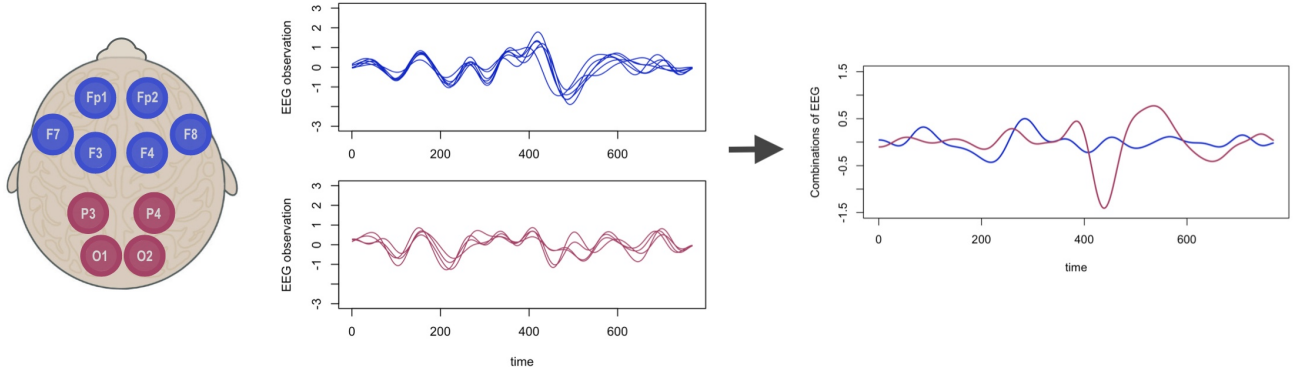


Figure 1: (Left) Blue colored nodes are channels on top of the frontal-prefrontal region and red colored nodes are channels on top of the occipital-parietal region. Multiple signals of Frontal-Prefrontal lobe EEG channels (mid-top) and that of Occipital-Parietal lobe EEG channels filtered at the Delta band (0,4)Hz. (Right) “Summary” signals representing EEG channels of Frontal-Prefrontal lobe and Occipital-Parietal lobe at the Delta band (0,4)Hz.

develop a novel procedure for identifying associations between oscillatory activity between groups of EEG channels that is robust to presence of outliers.

1.1 Spectral dependence

To characterize dependence between neuronal populations, our focus will be on the synchronization of oscillations from different brain regions or channels. Let $\mathbf{X}(t) = (X_1(t), \dots, X_p(t))^\top$, for $t = \{1, \dots, T\}$, be a collection of EEG signals from one group of channels, which we assume to be weakly stationary over time $t = 1, \dots, T$. The Cramér representation of $\mathbf{X}(t)$, in terms of the Fourier basis waveforms $\{\phi(\omega) = \exp(i2\pi\omega t), \omega \in (-\frac{1}{2}, \frac{1}{2})\}$, and complex-valued random amplitudes $\{d\mathbf{A}(\omega) = (dA_1(\omega), \dots, dA_p(\omega))^\top, \omega \in (-\frac{1}{2}, \frac{1}{2})\}$, is given by

$$\mathbf{X}(t) = \int_{-0.5}^{0.5} \phi(\omega) d\mathbf{A}(\omega),$$

The random coefficients satisfy $E[d\mathbf{A}(\omega)] = \mathbf{0}$, $\text{Cov}(d\mathbf{A}(\omega), d\mathbf{A}(\lambda)) = \mathbf{0}$ when $\lambda \neq \omega$ and

$$\text{Cov}(d\mathbf{A}(\omega), d\mathbf{A}(\omega)) = \mathbf{f}(\omega) d\omega, \quad (1)$$

where $\mathbf{f}(\omega)$ is the $p \times p$ spectral matrix which is Hermitian. The diagonal elements, $f_{jj}(\omega)$ for $j = 1, \dots, p$, are the auto-spectra and the off-diagonal elements, $f_{jk}(\omega)$ for $j \neq k = 1, \dots, p$, are the cross-spectra. Since $\mathbf{f}(\omega)$ is Hermitian, then $f_{jk}(\omega) = f_{kj}^*(\omega)$, where $f_{kj}^*(\omega)$ is the complex-conjugate

of $f_{jk}(\omega)$, for $j \neq k = 1, \dots, p$. We now define coherence which is a well-known measure of pairwise synchrony (Shumway et al., 2000; Brillinger, 2001). Coherence between channels p and q at frequency ω is

$$\begin{aligned}\rho_{jk}(\omega) &= \|\text{Cor}(dA_j(\omega), dA_k(\omega))\|^2 \\ &= \frac{|f_{jk}(\omega)|^2}{f_{jj}(\omega)f_{kk}(\omega)}.\end{aligned}\tag{2}$$

From Equation (2), we note that (a.) the spectral density matrix, $\mathbf{f}(\omega)$, captures the relative contribution of all oscillations to the total variance for each channel and (b.) coherence is a frequency-domain analogue of squared cross-correlation. An intuitive interpretation of coherence can be demonstrated under the framework in Ombao and Pinto (2022), as follows. Define the oscillatory component at frequency ω (henceforth referred to as ω -oscillation) at channel j to be $X_{j,\omega}(t) = \exp(i2\pi\omega t)dA_j(\omega)$, for $j = 1, \dots, p$. It turns out that coherence can be viewed as the squared correlation between these oscillations, i.e.,

$$\begin{aligned}\|\text{Cor}(X_{j,\omega}(t), X_{k,\omega}(t))\|^2 &= \|\text{Cor}(dA_j(\omega), dA_k(\omega))\|^2 \\ &= \rho_{jk}(\omega).\end{aligned}$$

Typically, in EEG analysis, coherence at a specific frequency *band* reveals more interpretation rather than at a singleton frequency. The standard frequency bands in EEG analysis are the delta (0, 4]Hz, theta (4, 8]Hz, alpha (8, 12]Hz, beta (12, 30]Hz and gamma (30, 50]Hz (Abhang and Mehrotra, 2016). In practice, coherence between a pair of channels is estimated by applying a bandpass filter (e.g., Butterworth filter, Daud and Sudirman, 2015). For sampling rate, S (i.e., S data points are observed per second), let $\Omega = \{S\omega : \omega \in [-\omega_1, -\omega_2] \cup [\omega_1, \omega_2]\}$ be a frequency band with $0 < \omega_1 < \omega_2 < 1/2$. The filtered signal at channel $X_j(t)$, denoted by $X_{j,\Omega}(t)$, is $X_{j,\Omega}(t) = \sum_{h=-\infty}^{\infty} c_h X_j(t-h)$, for $j = 1, \dots, p$. The function c_h is a linear filter, such that,

$$\left| \sum_{h=-\infty}^{\infty} c_h e^{-i2\pi\omega h} \right|^2 = \begin{cases} 1/2\delta & \text{for } \omega \in \Omega/S \\ 0 & \text{for } \omega \notin \Omega/S \end{cases}\tag{3}$$

where $\delta = \omega_2 - \omega_1$ is some constant (see [Ombao and Van Bellegem, 2008](#), for details). This yields to a filtered series $X_{j,\Omega}(t)$ with zero power-spectrum outside the frequency band Ω (see, e.g., [Ombao et al., 2006](#)). The coherence of channels j and k at frequency band Ω is then equal to

$$\rho_{jk}(\Omega) = \frac{|f_{jk}(\Omega)|^2}{f_{jj}(\Omega)f_{kk}(\Omega)}$$

$$f_{jk}(\Omega) = \int_{-0.5}^{0.5} f_{jk}^{(\Omega)}(\omega) \exp^{i\Phi_\omega} d\omega \quad \text{and} \quad f_{jj}(\Omega) = \int_{-0.5}^{0.5} f_{jj}^{(\Omega)}(\omega) d\omega \quad (4)$$

where $\Phi_\omega = 2\pi\omega h_0$ and h_0 is some lead-lag dependence between $X_{j,\Omega}(t)$ and $X_{k,\Omega}(t)$. This $\exp^{i\Phi_\omega}$ is the phase-shift or time-delay in the relationship of j -th and k -th channels as function of ω (for discussion of phase-shift, see [Shumway et al., 2000](#)). Moreover, $f_{jk}^{(\Omega)}(\omega)$ is the cross-spectrum density of $X_{j,\Omega}(t)$ and $X_{k,\Omega}(t)$, while $f_{jj}^{(\Omega)}(\omega)$ and $f_{kk}^{(\Omega)}(\omega)$ are the corresponding auto-spectra (note that $f_{kk}^{(\Omega)}(\omega)$ is defined similarly as $f_{jj}^{(\Omega)}(\omega)$). We can also view the spectral density of filtered series as,

$$f_{jk}^{(\Omega)}(\omega) = |C(\omega)|^2 f_{jk}(\omega) \quad (5)$$

where $C(\omega) = \sum_{h=-\infty}^{\infty} c_h \exp^{-i2\pi\omega h}$ is a symmetric frequency response function of the filter ([Lindgren et al., 2013](#); [Ombao and Pinto, 2022](#)). The above relation implies that the observed filtered signals can be used to estimate the coherence at each frequency band. Coherence is a frequency-based measure of dependence between two series.

Suppose now that the main interest is to characterize dependence between two sets of channels $\mathbf{X}(t) = (X_1(t), \dots, X_p(t))^\top$, and $\mathbf{Y}(t) = (Y_1(t), \dots, Y_q(t))^\top$, for $t = \{1, \dots, T\}$. A naive way is to characterize dependence between individual channels $(X_j(t), Y_k(t))$ where $j = 1, \dots, p$ and $k = 1, \dots, q$. However, such approach is not ideal since the pairwise measure does not capture the concurrent dependence among $\mathbf{X}(t)$ and $\mathbf{Y}(t)$. An alternative solution is ‘‘canonical coherence’’ developed by [Brillinger \(2001\)](#) which is the time-series analogue of older concept of canonical correlation by ([Hotelling, 1992](#)). We now describe the general idea of canonical coherence in the frequency-domain perspective. Suppose that $\mathbf{X}(t)$ and $\mathbf{Y}(t)$ are both zero-mean weakly stationary process which we concatenate into single $(p + q) \times 1$ vector, $\mathbf{Z}(t) = (X_1(t), \dots, X_p(t), Y_1(t), \dots, Y_q(t))^\top$. Denote the covariance matrix of $\mathbf{Z}(t)$ at lag h to be

$$\Sigma_{ZZ}(h) = \begin{pmatrix} \Sigma_{XX}(h) & \Sigma_{XY}(h) \\ \Sigma_{YX}(h) & \Sigma_{YY}(h) \end{pmatrix}.$$

The corresponding spectral matrix of $\mathbf{Z}(t)$ is

$$\mathbf{f}_{ZZ}(\omega) = \begin{pmatrix} \mathbf{f}_{XX}(\omega) & \mathbf{f}_{XY}(\omega) \\ \mathbf{f}_{YX}(\omega) & \mathbf{f}_{YY}(\omega) \end{pmatrix}.$$

where $\mathbf{f}_{XX}(\omega)$ is the $p \times p$ auto-spectral matrix of $\mathbf{X}(t)$, $\mathbf{f}_{YY}(\omega)$ is the $q \times q$ auto-spectral matrix of $\mathbf{Y}(t)$, and $\mathbf{f}_{XY}(\omega)$ is the $p \times q$ cross-spectral matrix between $\mathbf{X}(t)$ and $\mathbf{Y}(t)$. Given vectors $\mathbf{a} \in \mathbb{C}^p$ and $\mathbf{b} \in \mathbb{C}^q$, such that, $\mathbf{a}^\top \mathbf{f}_{XX}(\omega) \mathbf{a} = \mathbf{b}^\top \mathbf{f}_{YY}(\omega) \mathbf{b} = 1$, the canonical coherence at frequency ω (denoted as $\theta(\omega)$) was defined by Brillinger (2001) as,

$$\theta(\omega) = \max_{\forall \{\mathbf{a}, \mathbf{b}\}} \left| \frac{\mathbf{a}^\top \mathbf{f}_{XY}(\omega) \mathbf{b}}{\sqrt{\mathbf{a}^\top \mathbf{f}_{XX}(\omega) \mathbf{a} \mathbf{b}^\top \mathbf{f}_{YY}(\omega) \mathbf{b}}} \right|^2.$$

There are literature on the use of canonical coherence to study dependence between various modalities. Vidaurre et al. (2019) proposed to use the eigenvalue decomposition of the real part of cross-spectral matrix at a specific frequency ω , i.e., $Re(\mathbf{f}_{XY}(\omega))$. When we use only the real part of the spectral matrix, we ignore the imaginary components that contains the phase information that is part of the definition of the cross-spectral matrix (see the definition of $f_{jk}(\Omega)$ in Equation (4)). Hence, in their method, the authors develop a separate algorithm to detect this phase-shift. In our proposed method, we mitigate this problem by incorporating the phase-shift detection in the process. This phase-shift is related to the concept of lead-lag relationship between $\{X(t)\}_{t=1}^T$ and $\{Y(t)\}_{t=1}^T$, i.e., the maximum association among $\{X(t)\}_{t=1}^T$ and $\{Y(t)\}_{t=1}^T$ is not contemporaneous (Hause, 1971). In addition to this, current literature on canonical coherence depends on moment-based estimation of the covariance matrix (Brillinger, 2001; Vidaurre et al., 2019; Dehon et al., 2000). These estimators break down in the presence of outliers. To mitigate this problem, we develop a new characterization and estimation for canonical coherence that captures the monotonic dependence structure among the signals. Our measure is the first ranked-based canonical coherence that does not require the existence of second moment. Since the proposed measure of canonical coherence is based on Kendall's τ correlation coefficient, we refer it to as KenCoh.

In this paper, we demonstrate that the proposed KenCoh method is able to (a.) provide a robust and frequency-based global association measure between two sets of signals and (b.) to detect differences in connectivity structure during the two brain states in EEG (i.e., alert-state and drowsy-state).

1.2 Contributions

The main contribution of the proposed KenCoh is to provide a method for estimating canonical coherence between multivariate time series at given a frequency band. Moreover, we develop a statistical procedure to test the difference between pattern of connectivity at different states of the brain.

The key advantages of our proposed method are as follows:

1. It provides a “global” connectivity, not just for a single ω -frequency but for frequency-bands, Ω , that are linked to brain functionalities.
2. It is robust in the presence of outliers;
3. It serves as a basis of a powerful non-parametric hypothesis testing procedure; and
4. It equips with tools to develop a deeper understanding of the differences in brain networks (e.g., for alert and drowsy states during a virtual-driving experiment).

The rest of the article is organized as follows: in Section 2, we present the KenCoh method which is a new approach to estimating canonical coherence. In Section 3 we conduct simulation studies under various settings to investigate robustness of KenCoh and in Section 4, we report novel findings on a virtual-reality driving experiment dataset. Finally, Section 5 summarizes the conclusion of the study and limitations of the proposed method.

2 Methodology

Let $\{\mathbf{Z}(t)\}_{t=1}^T = \{X_1(t), \dots, X_p(t), Y_1(t), \dots, Y_q(t)\}_{t=1}^T$ as the concatenated vector of two regions. Moreover, let $Z_j^\Omega(t)$ denote the bandpass filtered $Z_j(t)$ at Ω -band for $j = 1, \dots, (d = p + q)$. Let $\mathfrak{p}(\cdot; \Omega, h)$ denote a monotonic spectral dependence function for $X^\Omega(t)$ and $Y^\Omega(t)$ at a specific Ω -band and lag h , for $h = 0, 1, \dots, L$. Further, we define the lagged cross-dependence matrix among filtered signals on Ω at lag h , $h = 0, 1, \dots, L$, as $\mathbf{P}(\Omega, h)$, such that,

$$P_{jk}(\Omega, h) := \mathfrak{p}(Z_j^\Omega(t-h), Z_k^\Omega(t)) = \mathfrak{p}(Z_j^\Omega(t), Z_k^\Omega(t+h))$$

for all $j, k = 1, \dots, (d = p + q)$. We define the four sub-matrices of $\mathbf{P}(\Omega, h)$ as,

$$\mathbf{P}(\Omega, h) = \begin{pmatrix} \mathbf{P}_{XX}(\Omega, h) & \mathbf{P}_{XY}(\Omega, h) \\ \mathbf{P}_{YX}(\Omega, h) & \mathbf{P}_{YY}(\Omega, h) \end{pmatrix}. \quad (6)$$

It is important to note here that $\mathbf{P}_{XY}(\Omega, h) = \mathbf{P}_{YX}(\Omega, -h)^\top$. If $\rho(\cdot)$ is the Pearson's correlation coefficient, then $\mathbf{P}(\Omega, h)$ is the matrix of coherency (see [Ombao and Pinto \(2022\)](#) for discussion of coherency). We are now ready to define canonical band-coherence in the context of linear filtering.

Definition 2.1 (Canonical Band-Coherence) Consider a weakly stationary time series, $\{X(t)\}_{t=1}^T = \{X_1(t), \dots, X_p(t)\}_{t=1}^T$, and, $\{Y(t)\}_{t=1}^T = \{Y_1(t), \dots, Y_q(t)\}_{t=1}^T$. Define $\mathbf{P}(\Omega, h)$ as the lagged cross-dependence matrix among filtered signals on Ω at lag h . We define canonical band-coherence between $\{\mathbf{X}(t)\}_{t=1}^T$ and $\{\mathbf{Y}(t)\}_{t=1}^T$, at specific Ω , denoted as $\kappa_{XY}(\Omega)$, where $\kappa_{XY}(\Omega) : \mathbb{R}^{p+q} \rightarrow \mathbb{R}^+$.

$$\kappa_{XY}(\Omega) := \max_{\forall \{\mathbf{u}_\Omega, \mathbf{v}_\Omega, h\}} \left\{ \mathbf{u}_\Omega^\top \mathbf{P}_{XY}(\Omega, h) \mathbf{v}_\Omega \right\}^2 \quad (7)$$

where $\mathbf{u}_\Omega \in \mathbb{R}^p$ and $\mathbf{v}_\Omega \in \mathbb{R}^q$ are vectors with dimensions $p \times 1$ and $q \times 1$, respectively.

The pre-multiplication and post-multiplication of vectors \mathbf{u}_Ω and \mathbf{v}_Ω , respectively, allow us to have a scalar value for $\kappa_{XY}(\Omega)$. This is subject to the constraint that $\mathbf{u}_\Omega^\top \mathbf{u}_\Omega = \mathbf{v}_\Omega^\top \mathbf{v}_\Omega = 1$ ([Mardia and Kent, 1979](#)). The vectors \mathbf{u}_Ω and \mathbf{v}_Ω are referred to as the *standardized canonical directions*.

Theorem 2.2 Define a weakly stationary time-series $\{\mathbf{Z}(t)\}_{t=1}^T = \{X_1(t), \dots, X_p(t), Y_1(t), \dots, Y_q(t)\}_{t=1}^T$ and a linear filter, c_h , defined in Equation 3. Let $\mathbf{Z}_\Omega(t)$ be the convolution of $\mathbf{Z}(t)$ and c_h . Further, we have $\mathbf{P}(\Omega, h)$ as the lagged dependence matrix of $\mathbf{Z}_\Omega(t)$ defined in Equation 6. If second-order moments of $\{\mathbf{Z}(t)\}_{t=1}^T$ exists, Eq. (7) is equivalent to,

$$\kappa_{XY}(\Omega) = \max_{\forall \{\mathbf{a}_\Omega, \mathbf{b}_\Omega, h\}} \left| \mathbf{a}_\Omega^\top \left[\int_{\Omega} \mathbf{f}_{XY}(\omega) \exp^{i2\pi\omega h} d\omega \right] \mathbf{b}_\Omega \right|^2$$

where $\mathbf{a}_\Omega = \mathbf{f}_{XX}(\Omega)^{-1/2} \mathbf{u}_\Omega$ and $\mathbf{b}_\Omega = \mathbf{f}_{YY}(\Omega)^{-1/2} \mathbf{v}_\Omega$.

The proof of Theorem 2.2 can be found in Appendix A. Theorem 2.2 shows that through linear filtering, we can maximize the integral of spectral density matrix corresponding to the band of interest. This theorem also shows that by finding the lead-lag that maximizes $\kappa_{XY}(\Omega)$, we are taking into account the

phase-shift of the oscillation, which in this case equivalent to $2\pi\omega h$. The solution to the maximization problem in Eq 7 can be obtained through solving for the eigenvalues and eigenvectors of,

$$\mathbf{P}_{XX}^{-1}(\Omega, 0)\mathbf{P}_{XY}(\Omega, h)\mathbf{P}_{YY}^{-1}(\Omega, 0)\mathbf{P}_{YX}(\Omega, -h) \quad (8)$$

$$\mathbf{P}_{YY}^{-1}(\Omega, 0)\mathbf{P}_{YX}(\Omega, -h)\mathbf{P}_{XX}^{-1}(\Omega, 0)\mathbf{P}_{XY}(\Omega, h) \quad (9)$$

Denote $\Lambda_j^{(x)}(\Omega, h)$ as the j -th largest eigenvalue of the matrix in Eq. (8) and $\Lambda_k^{(y)}(\Omega, h)$ as the k -th largest eigenvalues of Eq. (9) for $j, k = 1, \dots, \min(p, q)$. Let $\Lambda_1(\Omega, h) = \Lambda_1^{(x)}(\Omega, h) = \Lambda_1^{(y)}(\Omega, h)$ be the largest eigenvalue for a given lag h . It follows that the solution to the Equation 7 is

$$\kappa_{XY}(\Omega) = \max_{\forall h} \{\Lambda_1(\Omega, h)\}.$$

For each non-zero $\{\Lambda_j(\Omega)\}_{j=1}^{\min(p, q)}$, we have the corresponding j -th eigenvector of Eq. (8), which is the solution to the j -th standardized canonical direction of filtered $\mathbf{X}(t)$ at frequency band Ω , denoted as $\mathbf{u}_{\Omega}^{(j)} = \{u_{1, \Omega}^{(j)}, \dots, u_{p, \Omega}^{(j)}\}$. Correspondingly, we have the j -th eigenvector of Eq. (9) as the solution to the j -th standardized canonical direction of the filtered $\mathbf{Y}(t)$ at frequency band Ω , denoted as $\mathbf{v}_{\Omega}^{(j)} = \{v_{1, \Omega}^{(j)}, \dots, v_{q, \Omega}^{(j)}\}$ for $j = 1, \dots, \min(p, q)$. For brevity, we hereafter drop the superscript for the rank of direction, that is, we always refer to the first direction whenever we use \mathbf{u}_{Ω} and \mathbf{v}_{Ω} .

Eigenvalues and eigenvectors provide different lenses of connectivity. While the eigenvalues measures the maximum band-coherence between two sets of signals, the eigenvectors show the relative contribution of the channels to the overall association (see Figure 5 for illustration of eigenvectors). This paper focuses on the structure of connectivity between the two brain regions attributed to specific band-oscillation, and we develop a statistical procedure to test the difference between canonical directions.

2.1 Estimation

It is known that non-invasive brain imaging modalities are contaminated with noise (Yong et al., 2009). The standard estimators of the spectral and covariance matrices are sensitive to outliers and this can produce misleading results about the strength of the connectivity and the brain functional network captured by the eigenvalue and eigenvectors, respectively. To handle the outliers, we consider rank-

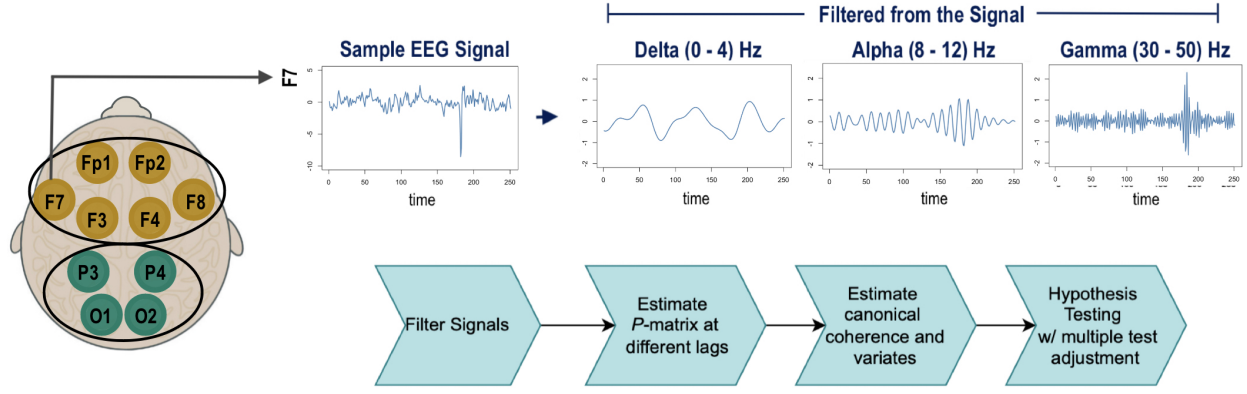


Figure 2: Framework of data analysis

based estimators. Here, we present the novel contribution of this paper which includes measures of characterizing channel contribution and estimation of dependency between two set of signals – that is, we generalize the concept of the classical canonical coherence by encompassing non-linear dependence and building on the robust approaches for dependence. We applied a ranked-based estimator which has desirable asymptotic properties for class of trans-elliptic distribution (Fang et al., 2002; Langworthy et al., 2021). Based on discussion above, $\rho(\cdot)$ can be considered as the Pearson’s correlation coefficient between filtered series. Here, the Pearson’s correlation coefficient can be estimated as,

$$\begin{aligned}\hat{C}_{jk}(\Omega, h) &= \frac{1}{T} \sum_{\forall t} (Z_j^\Omega(t) - \bar{Z}_j^\Omega)(Z_k^\Omega(t-h) - \bar{Z}_k^\Omega) \\ \hat{\rho}_{jk}(\Omega, h) &= \frac{\hat{C}_{jk}(\Omega, h)}{\sqrt{\hat{C}_{jj}(\Omega, h) \hat{C}_{kk}(\Omega, h)}}.\end{aligned}\quad (10)$$

where $\bar{Z}_j^\Omega = T^{-1} \sum_{\forall t} Z_j^\Omega(t)$ and similarly defined for \bar{Z}_k^Ω . We now define the statistic $\hat{P}_{jk}(\Omega, h)$ to estimate the j, k -th element of the matrix $\mathbf{P}(\Omega, h)$, for $j, k = 1, \dots, d$.

$$\hat{\tau}_{jk}(\Omega, h) = \frac{1}{\binom{T}{2}} \sum_{1 \leq t < s \leq T} \text{sign}\{(Z_j(t) - Z_j(s))(Z_k(t-h) - Z_k(s-h))\} \quad (11)$$

$$\hat{P}_{jk}(\Omega, h) = \sin\left(\frac{\pi}{2} \hat{\tau}_{jk}(\Omega, h)\right) \quad (12)$$

This estimator is particularly useful when second order moment of the signals does not exist.

The simulation studies compare the performance of this estimator to the usual estimator of coherency which we define in Eq 10. Provided the distribution is Gaussian, Pearson’s correlation

coefficient is a good candidate for estimation of $\mathbf{P}(\Omega, h)$. However, if there are outliers in the data, we expect this estimator to perform poorly.

2.2 Inference on connectivity using KenCoh

We propose here a hypothesis testing considering that there might be different conditions or states of the brain. One example is the data on virtual-reality driving experiment (Cao et al., 2019), where the goal is to compare two conditions/states of the brain, i.e., drowsy and alert. These kinds of experiments usually involve multiple independent trials to have replicates for the analysis. Each trial, b for $b = 1, \dots, B$, corresponds to a block of multivariate time series with sampling rate, S . A block, b , contains L number of time points. We denote a block of filtered multivariate time series as $\{\mathbf{Z}^\Omega(t)\}_{t \in \mathcal{T}_b}$ where $\mathcal{T}_b = \{(b-1)L+1, \dots, (b-1)L+L\}$, for $b = 1, \dots, B$. For each trial, b , we obtain the estimates of first canonical directions, $\hat{\mathbf{u}}_\Omega(b)$ and $\hat{\mathbf{v}}_\Omega(b)$. The blocks are labeled as either belonging to brain state 1, \mathcal{B}_1 , or brain state 2, \mathcal{B}_2 . Further, we assume that trials are independent.

Recall that the canonical directions defined in (7) is a measure of relative contribution of the channels to the maximal association. We now formulate a test for detecting differences in regional connectivity between the two brain states through the canonical directions. We consider the null hypothesis that there are no differences in the connectivity structure between the state 1 and state 2, or $\{\mathbf{u}_\Omega, \mathbf{v}_\Omega; \mathcal{B}_1\} = \{\mathbf{u}_\Omega, \mathbf{v}_\Omega; \mathcal{B}_2\}$. To measure the difference, we employed permutation test which uses the element-wise median of $\{\hat{\mathbf{u}}_\Omega(b), \hat{\mathbf{v}}_\Omega(b)\}_{b \in \mathcal{B}_g}$, for $g = 1, 2$. We then have $\hat{\mathbf{u}}_{j,\Omega}^{*(\mathcal{B}_g)} = \text{median}(\{\hat{u}_{j,\Omega}(b)\}_{b \in \mathcal{B}_g})$, for $j = 1, \dots, p$. Hence, the vector of median for $\hat{\mathbf{u}}_\Omega(b)$ given state- g is $\hat{\mathbf{u}}_\Omega^{*(\mathcal{B}_g)} = \{\hat{u}_{1,\Omega}^{*(\mathcal{B}_g)}, \dots, \hat{u}_{p,\Omega}^{*(\mathcal{B}_g)}\}$. Correspondingly, we have $\hat{\mathbf{v}}_\Omega^{*(\mathcal{B}_g)} = \{\hat{v}_{1,\Omega}^{*(\mathcal{B}_g)}, \dots, \hat{v}_{q,\Omega}^{*(\mathcal{B}_g)}\}$ as the vector of medians for the canonical directions of $\mathbf{Y}^{(\Omega)}(t)$. The test statistic, T_Ω , of the permutation test is as follows,

$$T_\Omega = \frac{\|\hat{\mathbf{u}}_\Omega^{*(\mathcal{B}_1)} - \hat{\mathbf{u}}_\Omega^{*(\mathcal{B}_2)}\|_{L_2}}{\sqrt{p}} + \frac{\|\hat{\mathbf{v}}_\Omega^{*(\mathcal{B}_1)} - \hat{\mathbf{v}}_\Omega^{*(\mathcal{B}_2)}\|_{L_2}}{\sqrt{q}}.$$

The empirical distribution of T_Ω , denoted as $\tilde{\mathbb{F}}_T$, under the null hypothesis is approximated in the process of permutation testing. We reject the null hypothesis if T_Ω is large, such that, $T_\Omega > \tilde{\mathbb{F}}^{-1}(1 - \alpha)$, where α is the level of significance. The p -value correction method proposed by Benjamini and Hochberg (2000) is used to adjust for multiple tests.

3 Simulation Study

In order to represent the five mutually-independent frequency bands (i.e., delta, theta, alpha, beta and gamma) of human EEG defined in Section 1.1, we use AR(2)-mixture model (Ombao and Pinto, 2022). In this section, we show the relationship of the canonical coherence and direction with the mixing-matrix of AR(2)-mixture model. We also provide the form of the spectral dependence function, $p(\cdot)$, of the AR(2)-mixture model in order to obtain the true canonical coherence and direction.

3.1 Simulation via AR(2) Mixture Model

In this section we demonstrate how we can represent the canonical coherence in a multivariate spectral model. EEGs are seen as superpositions of oscillations with random amplitudes. Since AR(2) processes represent oscillatory processes with specified frequency peak and bandwidth, they can be used as building blocks to simulated data (Gao et al., 2020; Granados-Garcia et al., 2022). We represent the jointly weakly-stationary time series within time block $\mathcal{T}_b = \{(b-1)L+1, \dots, (b-1)L+L\}$, for $b = 1, \dots, B$, using a mixture of AR(2) processes, given as,

$$\mathbf{Z}(t;b) = \begin{pmatrix} \mathbf{X}(t;b) \\ \mathbf{Y}(t;b) \end{pmatrix} = \mathbf{A}(t;b)\mathbf{O}(t;b) + \mathbf{W}(t;b) \quad \text{for } t \in \mathcal{T}_b, \quad (13)$$

where $\mathbf{Y}(t;b)$ as the data of dimension $1 \times q$ that are the sampled from q -channels at block b , and $\mathbf{X}(t;b)$ has dimension of $1 \times p$ which are from p -channels. $\mathbf{W}(t;b)$ are the white-noise processes, such that, e.g., $E[W_j(t;b)] = 0$ and $V[W_j(t;b)] = \sigma_W^2 < \infty, \forall j = 1, \dots, (d = p+q)$. $\mathbf{O}(t;b)$, with dimension 5×1 , are composed of $O_\ell(t;b)$ for $\ell = \{1, \dots, 5\}$, which are the independent Gaussian processes. Each of these $O_\ell(t;b)$ are modeled as AR(2) processes with peak of power spectrum at ω_ℓ and bandwidth of spectral density, M . In this setting, we fixed M to be the same for all $O_\ell(t;b)$. We have the parameters of these AR(2) processes to be equivalent to $\phi_1^{(\ell)} = 2\exp(-M)\cos(2\pi\omega_\ell)$; $\phi_2 = -\exp(-2M)$ Ombao and Pinto (2022), that is, $O_\ell(t) = \phi_1^{(\ell)}O_\ell(t-1) + \phi_2O_\ell(t-2) + \varepsilon_\ell(t)$; $\varepsilon_\ell(t) \stackrel{iID}{\sim} N(0, \sigma_\ell^2)$.

The theoretical spectral density function of $O_\ell(t;b)$ is $f_O^{(\ell)}(\omega_r) = \frac{\sigma_\ell^2}{|1 - \phi_1^{(\ell)}e^{-i2\pi\omega_r} - \phi_2e^{-i4\pi\omega_r}|^2}$, for $\ell = 1, \dots, 5$, $\omega_r = r/T$ and $r = 1, \dots, (T-1)$. The auto-spectra of the j -th EEG and the cross-spectra

between the j -th and k -th EEG are, respectively,

$$f_{jj}(\omega_r) = a_{j1}^2 f_O^{(1)}(\omega_r) + \dots + a_{j5}^2 f_O^{(5)}(\omega_r) + \sigma_W^2 \quad (14)$$

$$f_{jk}(\omega_r) = a_{j1} a_{k1} f_O^{(1)}(\omega_r) + \dots + a_{j5} a_{k5} f_O^{(5)}(\omega_r) \quad (15)$$

Further, we simulated $O_\ell(t; b)$ such that they are all mutually independent and are all independent from the noise. $\mathbf{A}(t; b)$ is constant within block b . The idea of simulation is to have two matrices, such that, $\{\mathbf{A}(t; b)\}_{b \in \mathcal{B}_1} := \mathbf{A}_1$ and $\{\mathbf{A}(t; b)\}_{b \in \mathcal{B}_2} := \mathbf{A}_2$. This produces two groups of multivariate time-series. Denote $a_{j\ell}$ as the elements of the \mathbf{A}_g matrix, for $g = 1, 2$, that has dimension $d \times 5$, for $j = 1, \dots, d$ and $\ell = 1, \dots, 5$. Using this simulation model, we have obtained the true form of band-specific spectral density matrix-function (see Eqs 4, 14 and 15), and hence the true values of canonical coherence ($\kappa_{XY}(\Omega)$) and canonical directions ($\{\mathbf{u}_\Omega, \mathbf{v}_\Omega\}$). Without loss of generality, we provide in Eq 16 the characteristic function for Eqs. (8) and (9) when $p = q = 2$. Let $c_\ell = f_O^{(\ell)}(\Omega)$, $k_1 = \frac{c_\ell \sigma_W^2}{(a_{1\ell}^2 c_\ell + \sigma_W^2)(a_{2\ell}^2 c_\ell + \sigma_W^2) - (a_{1\ell} a_{2\ell} c_\ell)^2}$, $k_2 = \frac{c_\ell \sigma_W^2}{(a_{3\ell}^2 c_\ell + \sigma_W^2)(a_{4\ell}^2 c_\ell + \sigma_W^2) - (a_{3\ell} a_{4\ell} c_\ell)^2}$, we obtain the eigenvalues of Eq. (8) by solving for λ in,

$$k_1 k_2 [(a_{1\ell}^2 a_{3\ell}^2 - a_{1\ell}^2 a_{4\ell}^2)(a_{2\ell}^2 a_{3\ell}^2 - a_{2\ell}^2 a_{4\ell}^2) \lambda^2 - (a_{1\ell} a_{2\ell} a_{3\ell}^2 - a_{1\ell} a_{1\ell} a_{4\ell}^2)^2] = 0 \quad (16)$$

From here, we see that the solutions are functions of only the \mathbf{A}_g matrix and the variance of white-noise was canceled-out along the process. Therefore, we may have a setting where $\mathbf{O}(t; b)$ is Gaussian and $\mathbf{W}(t; b)$ is Cauchy, and still retrieve the true values of canonical coherence and directions (Note: when $\mathbf{W}(t; b)$ is Cauchy then second-order moment does not exist). The white noise, $W_j(t; b)$, mimics a contamination in the sampling of signal or other irremovable artifacts from EEG recording.

3.2 Simulation Settings

In this paper, we provide three different settings for the white noise, $W_j(t; b) \quad \forall j = 1, \dots, d - (a)$: $W_j(t; b) \stackrel{iid}{\sim} N(0, 1)$; (b): $W_j(t; b) \stackrel{iid}{\sim}$ Student's $t_{(5)}$; (c): $W_j(t; b) \stackrel{iid}{\sim}$ Student's $t_{(1)}$. Note that the second-order moment of the Cauchy distribution does not exist. As described above, we have two types of $\{\mathbf{A}(t; b)\}_{t \in T}$ for $b \in \mathcal{B}_g$, that we denote as \mathbf{A}_g 's for $g = 1, 2$. This represents the signals for the two states, say drowsy (\mathcal{B}_1) and alert states (\mathcal{B}_2). To measure the effect size between the two states, Δ_ℓ , we obtain the L_2 -norm of true eigenvectors, that is, $\Delta_\ell = \frac{\|\mathbf{u}_{\Omega_\ell}^{(\mathcal{B}_1)} - \mathbf{u}_{\Omega_\ell}^{(\mathcal{B}_2)}\|_{L_2}}{\sqrt{p}} + \frac{\|\mathbf{v}_{\Omega_\ell}^{(\mathcal{B}_1)} - \mathbf{v}_{\Omega_\ell}^{(\mathcal{B}_2)}\|_{L_2}}{\sqrt{q}}$.

Table 1: Comparison of the power of the test in rejecting the null hypothesis that state 1 and state 2 directions are equal; using the ranked-based measure (\hat{P}_{xy}) estimator and using the usual estimator of variance-covariance matrix ($\hat{\rho}_{xy}$); Note: Δ is the difference between eigenvectors of state 1 and state 2.

Frequency Bands	Theta	Beta	Delta	Alpha	Gamma
Ground truth Δ	1.95	1.41	0.91	0.48	0
Purely Gaussian White Noise					
Test with traditional estimator, $\hat{\rho}_{xy}$	1.0	1.0	1.0	0.19	0
Test with Kencoh, \hat{P}_{xy}	1.0	1.0	1.0	0.42	0.03
Student's t-distributed (df=5) White Noise					
Test with traditional estimator, $\hat{\rho}_{xy}$	1.0	1.0	1.0	0.39	0.05
Test with Kencoh, \hat{P}_{xy}	1.0	1.0	1.0	0.43	0.02
Student's t-distributed (df=1) White Noise					
Test with traditional estimator, $\hat{\rho}_{xy}$	1.0	0.19	0.19	0.19	0
Test with Kencoh, \hat{P}_{xy}	1.0	1.0	1.0	0.55	0.04

In the simulated examples, we used five latent AR(2) processes for the (1) Delta-band(0-4) Hz; (2) Theta-band (4-8) Hz; (3) Alpha-band (8-12) Hz; (4) Beta-band (12-30) Hz; (5) Gamma-band (30-50) Hz. These five latent processes, $\mathbf{O}(t; b)$, are simulated to have $M = 1.05$ and peaks at $\omega_\ell = \{2, 6, 10, 25, 40\}$. We constructed \mathbf{A}_g so that the $\Delta = \{0.91, 1.95, 0.48, 1.41, 0\}$ for the five frequency bands, respectively. Hence, delta, theta and beta bands indicate high effect size ($\Delta_\ell > 0.5$) and alpha-band should give weak effect size ($\Delta_\ell \leq 0.5$). The gamma-band is used to quantify the size of the test $\Delta_\ell = 0$.

Following the setting of data from [Cao et al. \(2019\)](#), we have set the sampling rate to 128Hz for a 3-sec non-overlapping blocks. A single block, then, consists of 384 time points. We used 300 simulated blocks (50% for state 1 and another half for state 2) – yielding a data with dimension of $115,200 \times d$ where $d = 10$ (i.e., $p = 6, q = 4$).

3.3 Simulation Results

For power analysis, we replicated the estimation and testing procedure multiple times using (1) the standard estimator defined in Eq 10, hereafter regarded as VCov, and that of using (2) the KenCoh (Eq 12). The results are summarized in Table 1. For purely Gaussian distributed variables, tests using VCov accurately identify strong differences such as delta-band, theta-band and beta-band (i.e., $\Delta_\ell > 0.5, \forall \ell$), however, it has high false positives in weak differences like alpha-band with $\Delta_\ell = 0.48$

(i.e., failing to reject the null). On the other hand, tests using KenCoh have more powerful tests even for weak differences (i.e., $\Delta_\ell > 0, \forall \ell$).

We observed similar results for Student's t white noise with 5 degrees of freedom. For noise with heavy-tailed margins and non-existence of second-order moment, i.e., Cauchy distribution, we see big difference in the performance of VCov and KenCoh. The estimator using VCov is less powerful in identifying differences between two states, i.e., VCov has higher false positives for heavy-tailed settings. The power of test using KenCoh, on the other hand, is consistently powerful for $\Delta > 0.5$ and is correctly-sized.

4 Analysis of the Driving EEG Data

The goal of this paper is to develop a robust statistical tool for comparing dependence between two regions and identify differences between the alert ($g = 1$) vs drowsy ($g = 2$) states. Artifacts in EEG can contaminate the gamma-band (30-50)Hz (Muthukumaraswamy, 2013). This can also be observed in EEG plot of Figure 2 – a sample EEG recording of an alert individual at one frontal channel (F7). Figure 3 also shows sample trial from alert and drowsy states from a single subject. From these figures, we can see that signals are heavy-tailed and justifies the use of KenCoh. Figure 4 shows difference in the results of KenCoh and traditional method (VCov). VCov suggests significant differences in the gamma-band and this is mainly due to the weight given to F7 (VCov = -0.28, KenCoh = -0.13). From Figure 2, we can see that F7 has extreme values (potentially artifacts) that contaminates the gamma-band. Moreover, KenCoh detects significant difference between alert and drowsy states at high frequency band (i.e., beta-band). Beta-band is known to be linked with concentration (Srinivasan, 2007), hence differences in this bands for alert- and drowsy-state is reasonable.

Figure 5 shows the median values across the blocks of "global" association estimates by KenCoh as well as the weights attributed to frontal-prefrontal channels and occipital-parietal channels, i.e., $\{\hat{u}_\ell, \hat{v}_\ell\}$, for both drowsy and alert states. The direction represents the flow of information, i.e., we provide the summary of the overall association between the past/lag values of frontal-prefrontal channels and current values of the occipital-parietal channels. We observe that alert-state has stronger magnitude of weights for the frontal-prefrontal lobe at beta band. On the other hand, channels in the drowsy-state seem to provide a more equalized contributions to the global-association. Hence, in the alert-state of beta band (which is linked to concentration), there are channels that are superior with regards to the

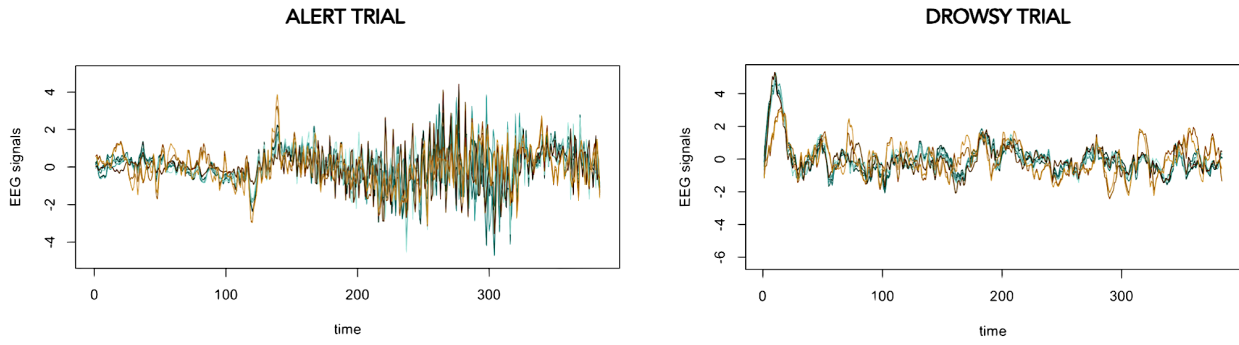


Figure 3: EEG signals at the frontal-prefrontal lobe (blue) and occipital-parietal lobe (brown) regions for one trial in alert state and drowsy state

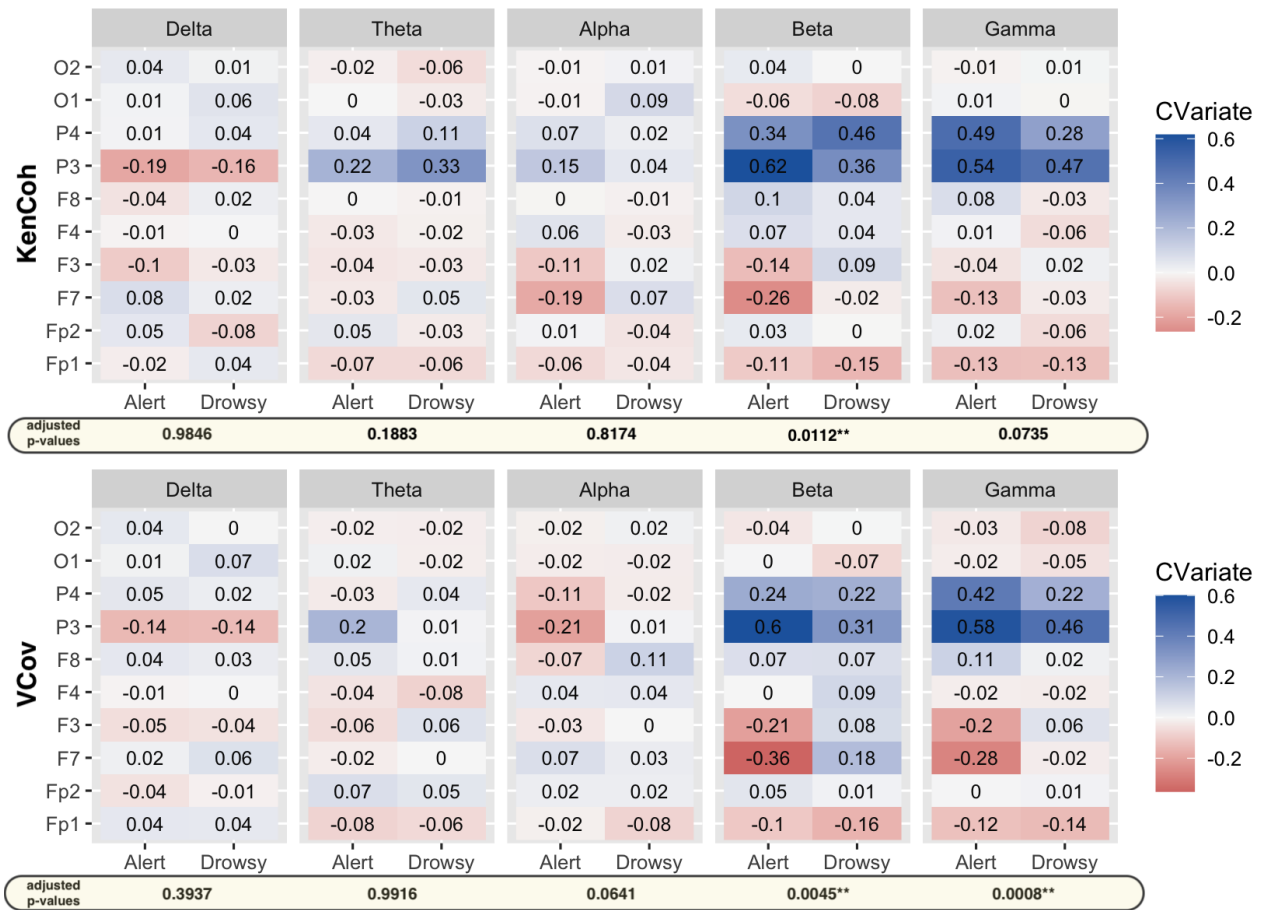


Figure 4: Median spectral canonical directions ($\hat{u}_{(M)}$ and $\hat{v}_{(M)}$) for frontal-prefrontal lobe and occipital-parietal lobe for alert and drowsy states of five frequency bands; comparing of results of KenCoh (top row) and VCov (bottom row). The p-values are adjusted using Benjamini and Hochberg (2000) adjustment

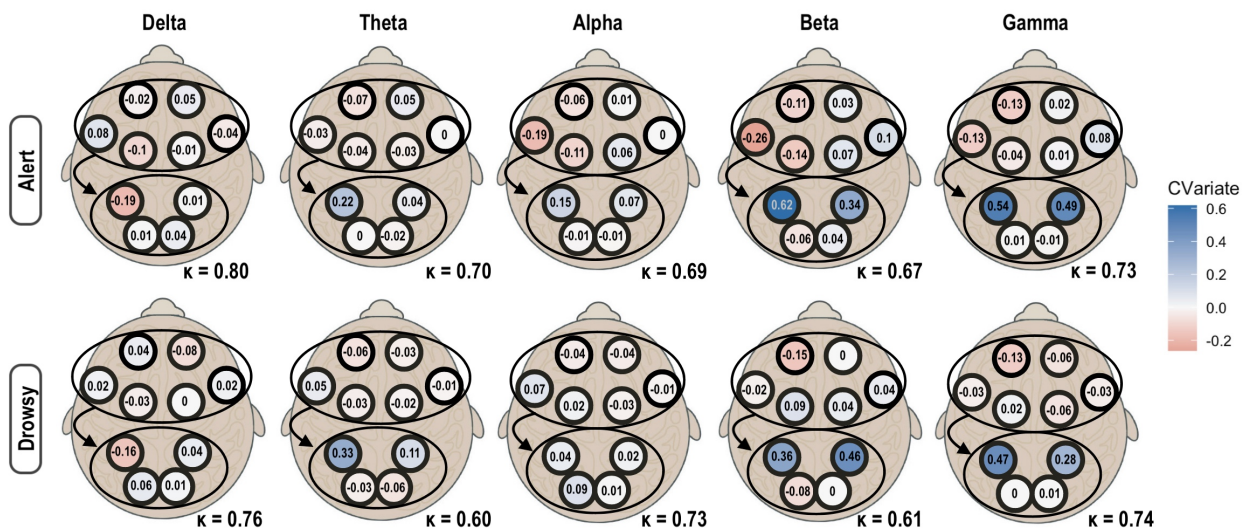


Figure 5: Median KenCoh spectral canonical directions ($\hat{\mathbf{u}}_{(M)}$ and $\hat{\mathbf{v}}_{(M)}$) for frontal-prefrontal lobe and occipital-parietal lobe for alert and drowsy states of five frequency bands

connection of frontal and occipital-parietal lobes. [Cole et al. \(2013\)](#) states that fronto-parietal brain network is the headquarter during “cognitive and task implementation”, hence, high activity during alert state at frontal lobe is sensible.

Zooming in further, larger weights are given to the left-hemisphere-frontal lobe and the parietal channels. [Yantis et al. \(2002\)](#) and [Liu et al. \(2023\)](#) reveal that fronto-parietal connection at the beta-band is related to active thinking. [Liu et al. \(2023\)](#) also mentioned that the right-frontal lobe is sensitive to distractions during beta-band. This interestingly complements our result of having relatively higher magnitude of weights given to left-frontal channels at beta-band of alert state. Moreover, the parietal lobe, which is responsible for spatial-orientation and perception, has higher weights in beta-band of alert-state. Since the data is driving experiment, and the result indicates the global association during alert state is mainly attributed to the sense of perception (parietal region) and cognition (frontal region) – a connection that is barely seen in the drowsy state.

5 Conclusion

The overall goal of this study is to develop a robust estimator and hypothesis testing for canonical coherence analysis. Our main advantage is by having a non-linear overall association among the oscillatory band-activity of signals that does not require the existence of the second moment. In addition to this, the novel elements of KenCoh include giving (robust measure of) weights to the

channels that builds a connectivity network among groups of signals. Through the powerful hypothesis testing that we built for Kencoh, we uncovered interesting and novel findings in the analysis of the EEG driving data. One of these is the stronger contribution of left-frontal lobe and parietal channels during alert state of beta band. This unique connection is the same connection mentioned in the literature when an individual is doing a physical activity (Liu et al., 2023; Yantis et al., 2002). The work presented here is limited to multiple independent trials of multivariate time-series, although this is the usual set-up of experimental studies. Future direction of this work will look into potential Markovian dependence of trials which is applicable when trials has sequencing.

A Appendix

Proof of Theorem 2.2

Let $\Sigma_{XY,\Omega}(h)$ be the covariance matrix of filtered series $\mathbf{X}^\Omega(t)$ and $\mathbf{Y}^\Omega(t)$ at band- Ω and lag- h , for $h = 0, 1, \dots, T-1$. Moreover, let $\Sigma_{XX,\Omega}$ and $\Sigma_{YY,\Omega}$ be the covariance matrix of filtered series $\mathbf{X}^\Omega(t)$ and $\mathbf{Y}^\Omega(t)$ at $h = 0$, respectively. If we let $\mathbf{P}_{XY}(\Omega, h)$ to be the correlation matrix, we have $\mathbf{P}_{XY}(\Omega, h) = \Sigma_{XX,\Omega}^{-1/2\top} \Sigma_{XY,\Omega} \Sigma_{YY,\Omega}^{-1/2}$. Given $\mathbf{a} = \Sigma_{XX,\Omega}^{-1/2} \mathbf{u}_\Omega$ and $\mathbf{b} = \Sigma_{YY,\Omega}^{-1/2} \mathbf{v}_\Omega$, such that, $\mathbf{u}_\Omega^\top \mathbf{u}_\Omega = \mathbf{v}_\Omega^\top \mathbf{v}_\Omega = 1$ then $\mathbf{a}^\top \Sigma_{XX,\Omega} \mathbf{a} = \mathbf{b}^\top \Sigma_{YY,\Omega} \mathbf{b} = 1$, and,

$$\begin{aligned} \kappa_{XY}^{1/2}(\Omega) &= \max_{\forall \{\mathbf{u}_\Omega, \mathbf{v}_\Omega; h\}} \mathbf{u}_\Omega^\top \Sigma_{XX,\Omega}^{-1/2\top} \Sigma_{XY,\Omega}(h) \Sigma_{YY,\Omega}^{-1/2} \mathbf{v}_\Omega \\ &= \max_{\forall \{\mathbf{a}, \mathbf{b}; h\}} \frac{\mathbf{a}^\top \Sigma_{XY,\Omega}(h) \mathbf{b}}{\sqrt{\mathbf{a}^\top \Sigma_{XX,\Omega} \mathbf{a} \mathbf{b}^\top \Sigma_{YY,\Omega} \mathbf{b}}} \end{aligned}$$

Given a filtered series $X^\Omega(t) = \sum_{h=-\infty}^{\infty} c_h X(t-h)$, where c_h is a linear filter that has zero spectrum outside a defined band, e.g., $|C(\omega)|^2 = |\sum_h c_h \exp^{-i2\pi\omega h}|^2 = 1/2\delta$ for $\omega \in \Omega/S$ and 0 otherwise (Ombao and Van Bellegem, 2008). Then $f_X(\Omega) = |C(\omega)|^2 f_X(\omega)$ Lindgren et al. (2013) and $\text{Cov}(X(t-h), X(t)) = \int_{-0.5}^{0.5} f_X(\omega) \exp^{i2\pi\omega h} d\omega$. Hence,

$$\begin{aligned} \kappa_{XY}^{1/2}(\Omega) &= \max_{\forall \{\mathbf{a}, \mathbf{b}; h\}} \frac{\mathbf{a}^\top \int_{-0.5}^{0.5} |C(\omega)|^2 \mathbf{f}_{XY}(\omega) \exp^{i2\pi\omega h} d\omega \mathbf{b}}{\sqrt{\mathbf{a}^\top \int_{-0.5}^{0.5} |C(\omega)|^2 \mathbf{f}_{XX}(\omega) d\omega \mathbf{a} \mathbf{b}^\top \int_{-0.5}^{0.5} |C(\omega)|^2 \mathbf{f}_{YY}(\omega) d\omega \mathbf{b}}} \\ &= \max_{\forall \{\mathbf{a}, \mathbf{b}; h\}} \frac{\mathbf{a}^\top \int_{\Omega} \mathbf{f}_{XY}(\omega) \exp^{i2\pi\omega h} d\omega \mathbf{b}}{\sqrt{\mathbf{a}^\top \mathbf{f}_{XX}(\Omega) \mathbf{a} \mathbf{b}^\top \mathbf{f}_{YY}(\Omega) \mathbf{b}}} \end{aligned}$$

Given $\mathbf{a}^\top \mathbf{f}_{XX}(\Omega) \mathbf{a} = \mathbf{b}^\top \mathbf{f}_{YY}(\Omega) \mathbf{b} = 1$, we have

$$\kappa_{XY}(\Omega) = \max_{\forall \{\mathbf{u}_\Omega, \mathbf{v}_\Omega; h\}} \left| \mathbf{u}^\top \Omega \mathbf{f}_{XX}(\Omega)^{-1/2} \left[\int_{\Omega} \mathbf{f}_{XY}(\omega) \exp^{i2\pi\omega h} d\omega \right] \mathbf{f}_{YY}(\Omega)^{-1/2} \mathbf{v}_\Omega \right|^2$$

□

References

- Abhang, P. and Mehrotra, S. (2016). *Technological Basics of EEG Recording and Operation of Apparatus*, pages 19–50.
- Bastos, A. M. and Schoffelen, J.-M. (2016). A tutorial review of functional connectivity analysis methods and their interpretational pitfalls. *Frontiers in Systems Neuroscience*, 9:175.
- Benjamini, Y. and Hochberg, Y. (2000). On the adaptive control of the false discovery rate in multiple testing with independent statistics. *Journal of Educational and Behavioral Statistics*, 25(1):60–83.
- Brillinger, D. R. (2001). *Time Series: Data Analysis and Theory*. SIAM.
- Cao, Z., Chuang, C.-H., King, J.-K., and Lin, C.-T. (2019). Multi-channel EEG recordings during a sustained-attention driving task. *Scientific Data*, 6(1):19.
- Cole, M. W., Reynolds, J. R., Power, J. D., Repovs, G., Anticevic, A., and Braver, T. S. (2013). Multi-task connectivity reveals flexible hubs for adaptive task control. *Nature Neuroscience*, 16(9):1348–1355.
- Daud, S. and Sudirman, R. (2015). Butterworth bandpass and stationary wavelet transform filter comparison for electroencephalography signal. In *2015 6th International Conference On Intelligent Systems, Modelling and Simulation*, pages 123–126. IEEE.
- Dehon, C., Filzmoser, P., and Croux, C. (2000). Robust methods for canonical correlation analysis. In *Data Analysis, Classification, and Related Methods*, pages 321–326. Springer.
- Fang, H.-B., Fang, K.-T., and Kotz, S. (2002). The meta-elliptical distributions with given marginals. *Journal of multivariate analysis*, 82(1):1–16.

- Gao, X., Shen, W., Shahbaba, B., Fortin, N. J., and Ombao, H. (2020). Evolutionary state-space model and its application to time-frequency analysis of local field potentials. *Statistica Sinica*, 30(3):1561.
- Granados-Garcia, G., Fiecas, M., Babak, S., Fortin, N. J., and Ombao, H. (2022). Brain waves analysis via a non-parametric bayesian mixture of autoregressive kernels. *Computational Statistics & Data Analysis*, 174:107409.
- Hause, J. C. (1971). Spectral analysis and the detection of lead-lag relations. *The American Economic Review*, 61(1):213–217.
- Hotelling, H. (1992). Relations between two sets of variates. In *Breakthroughs in statistics: methodology and distribution*, pages 162–190. Springer.
- Langworthy, B. W., Stephens, R. L., Gilmore, J. H., and Fine, J. P. (2021). Canonical correlation analysis for elliptical copulas. *Journal of Multivariate Analysis*, 183:104715.
- Lindgren, G., Rootzén, H., and Sandsten, M. (2013). *Stationary Stochastic Processes for Scientists and Engineers*. CRC press.
- Liu, R., Qi, S., Hao, S., Lian, G., and Luo, Y. (2023). Using electroencephalography to analyse drivers' different cognitive workload characteristics based on on-road experiment. *Frontiers in Psychology*, 14:1107176.
- Mardia, K. and Kent, J. (1979). *Multivariate analysis*. New York: Academic Press.
- Muthukumaraswamy, S. D. (2013). High-frequency brain activity and muscle artifacts in meg/eeg: a review and recommendations. *Frontiers in Human Neuroscience*, 7:138.
- Ombao, H. and Pinto, M. (2022). Spectral dependence. *Econometrics and Statistics*.
- Ombao, H. and Van Bellegem, S. (2008). Evolutionary coherence of nonstationary signals. *IEEE Transactions on Signal Processing*, 56(6):2259–2266.
- Ombao, H., Van Bellegem, S., et al. (2006). Coherence analysis of nonstationary time series: a linear filtering point of view. *IEEE Transactions on Signal Processing*, 56:2259–2266.
- Shi, C., Yan, F., Zhang, J., Yu, H., Peng, F., and Yan, L. (2023). Right superior frontal involved in distracted driving. *Transportation Research Part F: Traffic Psychology and Behaviour*, 93:191–203.

- Shumway, R. H., Stoffer, D. S., and Stoffer, D. S. (2000). *Time Series Analysis and its Applications*, volume 3. Springer.
- Spiers, H. J. and Maguire, E. A. (2007). Neural substrates of driving behaviour. *Neuroimage*, 36(1):245–255.
- Srinivasan, N. (2007). Cognitive neuroscience of creativity: EEG based approaches. *Methods*, 42(1):109–116.
- Vecino-Ortiz, A. I., Nagarajan, M., Elaraby, S., Guzman-Tordecilla, D. N., Paichadze, N., and Hyder, A. A. (2022). Saving lives through road safety risk factor interventions: global and national estimates. *The Lancet*, 400(10347):237–250.
- Vidaurre, C., Nolte, G., de Vries, I. E., Gómez, M., Boonstra, T. W., Müller, K.-R., Villringer, A., and Nikulin, V. V. (2019). Canonical maximization of coherence: a novel tool for investigation of neuronal interactions between two datasets. *Neuroimage*, 201:116009.
- Yantis, S., Schwarzbach, J., Serences, J. T., Carlson, R. L., Steinmetz, M. A., Pekar, J. J., and Courtney, S. M. (2002). Transient neural activity in human parietal cortex during spatial attention shifts. *Nature Neuroscience*, 5(10):995–1002.
- Yong, X., Ward, R. K., and Birch, G. E. (2009). Artifact removal in EEG using morphological component analysis. In *2009 IEEE International Conference on Acoustics, Speech and Signal Processing*, pages 345–348. IEEE.